

Exotic Hydrogen Bonding in Compressed Ammonia Hydrides

Xianqi Song,^{†,□} Ketao Yin,^{†,□,ID} Yanchao Wang,^{†,ID} Andreas Hermann,^{‡,ID} Hanyu Liu,^{†,ID} Jian Lv,^{†,ID} Quan Li,^{*,†,ID} Changfeng Chen,^{*,§} and Yanming Ma^{*,†,ID}

[†]State Key Laboratory of Superhard Materials, Key Laboratory of Automobile Materials of MOE, Department of Materials Science, and Innovation Center for Computational Physics Methods and Software, Jilin University, Changchun 130012, China

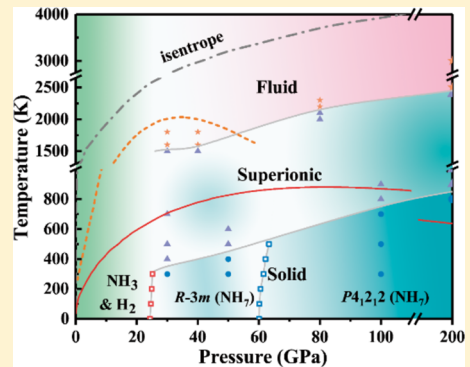
[‡]Centre for Science at Extreme Conditions and SUPA, School of Physics and Astronomy, The University of Edinburgh, Edinburgh EH9 3FD, United Kingdom

[§]International Center of Future Science, Jilin University, Changchun 130012, China

^{*}Department of Physics and Astronomy, University of Nevada, Las Vegas, Nevada 89154, United States

Supporting Information

ABSTRACT: Hydrogen-rich compounds attract significant fundamental and practical interest for their ability to accommodate diverse hydrogen bonding patterns and their promise as superior energy storage materials. Here, we report on an intriguing discovery of exotic hydrogen bonding in compressed ammonia hydrides and identify two novel ionic phases in an unusual stoichiometry NH_7 . The first is a hexagonal $R\bar{3}m$ phase containing $\text{NH}_3-\text{H}^+-\text{NH}_3$, H^- , and H_2 structural units stabilized above 25 GPa. The exotic $\text{NH}_3-\text{H}^+-\text{NH}_3$ unit comprises two NH_3 molecules bound to a proton donated from a H_2 molecule. Above 60 GPa, the structure transforms to a tetragonal $P4_12_12$ phase comprising NH_4^+ , H^- , and H_2 units. At elevated temperatures, fascinating superionic phases of NH_7 with part-solid and part-liquid structural forms are identified. The present findings advance fundamental knowledge about ammonia hydrides at high pressure with broad implications for studying planetary interiors and superior hydrogen storage materials.



Hydrogen-rich compounds have long been the subject of intense research efforts for fundamental scientific interests and practical application potentials, for example, as premier prototypes of efficient hydrogen storage media.^{1–5} Among such compounds, group V hydrides, e.g., ammonia (NH_3), hydrazine (N_2H_4), and hydrazoic acid (HN_3), are of particular interest for their ability to form special hydrogen bonding and flexible nitrogen backbone chains.^{6–8} Extensive theoretical and experimental studies^{5,9–14} have identified group V hydrides with intriguing chemical bonding patterns^{15–19} and high energy density. Used as rocket fuel, hydrazine has a very high hydrogen capacity of 12.6 wt %, and recent results show that the efficiency of hydrazine decomposition for hydrogen generation at room temperature can be improved by using group VIII metal-based catalysts.²⁰ Meanwhile, ammonia possesses even higher hydrogen capacity (17.6 wt %), making it a prototypical compound for research and development,²¹ especially as a prominent choice for hydrogen storage media supported by well-developed technologies for its synthesis and distribution as well as its easy catalytic decomposition.²² Ammonia is known to undergo phase transformations from molecular hydrogen-bonded to ionic nonhydrogen-bonded configurations.²¹ Ammonia and hydrogen are among the major constituents in the interior of giant planets Uranus and Neptune.²³ While ammonia is a unique solvent in terms of its ability to dissolve all the alkali metals,²⁴ there is no

experimental or theoretical evidence of chemical reactions between ammonia and hydrogen molecules.²⁵ Such reactions, however, may occur under high pressure conditions inside the giant planets, and the process and resulting products can be probed computationally and accessed by laboratory experiments, which may well unveil novel structural and chemical properties of ammonia hydrides. It is widely recognized that subtle bonding differences in hydrogen-rich compounds can have considerable influence on their stability and physical and chemical behavior. In this work, we explore possible new high-pressure forms of ammonia hydrides with novel bonding configurations and properties. The results may have implications for developing superior hydrogen storage media and shed light on the fundamental principles for understanding the physics and chemistry of giant planetary interiors.

We studied the stability of ammonia hydrides over a wide range of stoichiometry by calculating their formation enthalpy relative to that of the dissociation products of solid NH_3 and H_2 at 50, 100, and 200 GPa. The formation enthalpy of the NH_3-H_2 system is defined as $\Delta H = H(\text{N}_x\text{H}_{3x+2y}) - xH(\text{NH}_3) - yH(\text{H}_2)$, where the most stable $P2_12_12$ and $Pma2$ phases of NH_3 and the $P6_3/m$ and $C2/c$ phases of H_2 at the

Received: April 5, 2019

Accepted: May 8, 2019

Published: May 8, 2019

corresponding pressures were chosen as the reference phases.^{26,27} The calculated convex hulls (Figure 1a) show

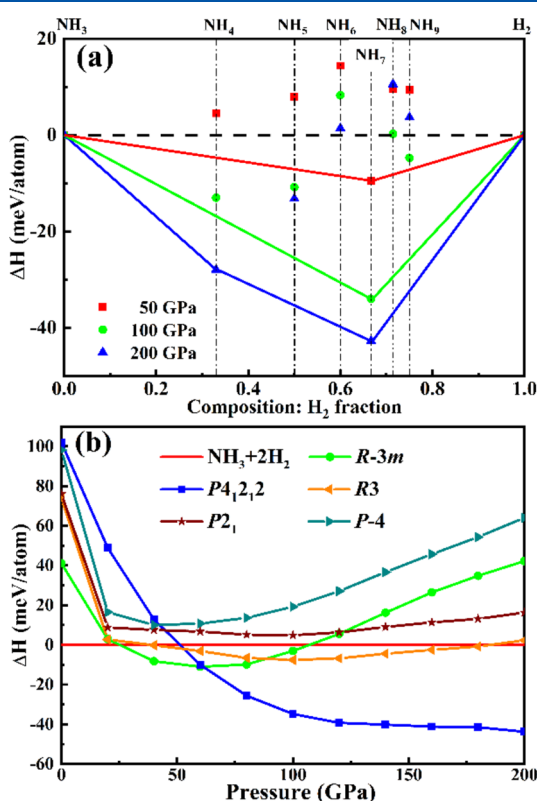


Figure 1. (a) Calculated formation enthalpy of various $\text{NH}_3\text{-H}_2$ compounds with respect to the decomposition. The convex hulls are indicated by solid lines. (b) Calculated enthalpy of the predicted NH_7 phases relative to that of the decomposition products in 0–200 GPa.

that among the studied $\text{NH}_3\text{-H}_2$ structures, NH_7 is the only compound that is stable against decomposition in the wide pressure range examined; note that the onset of stability of NH_4 is delayed to 125 GPa due to the emergence of the new NH_7 compound.⁵ We refined our formation enthalpy calculations for various NH_7 phases relative to NH_3 and H_2 in 0–200 GPa. At about 25 GPa, a hexagonal structure in $\bar{R}\bar{3}m$ symmetry becomes more stable than the NH_3 and H_2 mixture (Figure 1b). This structure has a gravimetric density of 33.3 wt % hydrogen storage capacity, and 19.0 wt % is extractable upon decomposition into NH_3 and H_2 , which represent the highest hydrogen storage and releasing capacity among all known materials. The $\bar{R}\bar{3}m$ NH_7 phase adopts a sixfold symmetry and comprises intriguing $\text{NH}_3\text{-H-NH}_3$, H_2 , and H^- units (Figure 2). In this ammonia hydride structure, each ionic H^- is surrounded by six H_2 at an equal distance of 1.761 Å; it is located at the central sites of the six $\text{NH}_3\text{-H-NH}_3$ units. At increasing pressures, the $\bar{R}\bar{3}m$ structure undergoes a phase transition at 60 GPa to a tetragonal $P4_12_2$ structure, which consists of tetrahedral NH_4^+ , H_2 , and H^- units, where each H^- unit is surrounded by three tetrahedral NH_4^+ and three H_2 units occupying the interstitial regions and forming a spiral pipe structure. More structural information is presented in the Supporting Information (Table S1 and Figure S1).

We examined the effects of the van der Waals interactions and zero-point energy on the stability of compressed ammonia hydrides.²⁸ The results (Figure S2) show that these effects shift

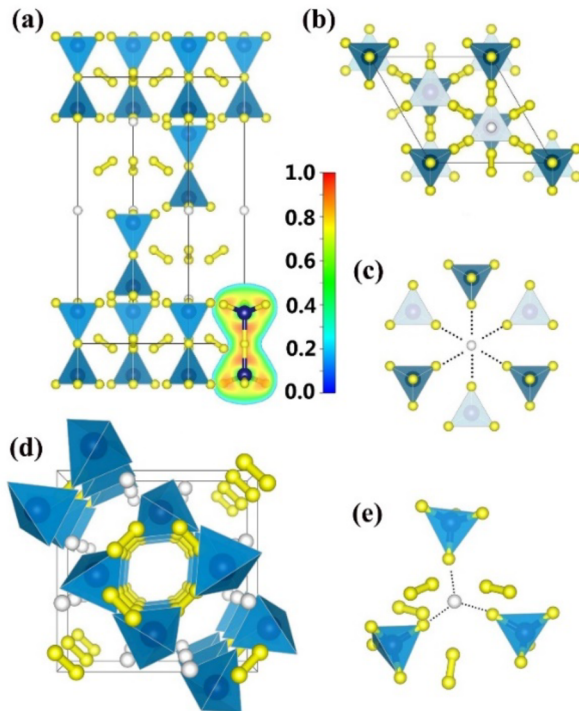


Figure 2. (a) Polyhedral and (b) top view of the $\bar{R}\bar{3}m$ structure of NH_7 at 50 GPa with the ELF plot of the $\text{NH}_3\text{-H-NH}_3$ unit shown in panel a. (c) Hydrogen bonds between the ionic H^- and $\text{NH}_3\text{-H}^+-\text{NH}_3$ units. (d) Top view of the crystal structure in $P4_12_2$ symmetry at 100 GPa. (e) Ionic bonding characters between the ionic H^- and NH_4^+ units. Blue, yellow, and white spheres represent nitrogen, hydrogen, and ionic hydrogen atoms, respectively.

the calculated enthalpy values downward but do not change their relative order. We also calculated phonon dispersions²⁹ and observed no imaginary frequencies (Figure S3), which indicates that these NH_7 phases are dynamically stable. The calculated electronic band structures (Figure S4) show that NH_7 is a semiconductor with an indirect band gap of 2.4 eV ($\bar{R}\bar{3}m$ phase) at 50 GPa and 1.2 eV ($P4_12_2$ phase) at 100 GPa, in sharp contrast to solid ammonia that remains an insulator with a large band gap of 5.3 eV at 100 GPa.²⁶ Moreover, we performed calculations to determine the structural stability of the NH_7 phases at finite temperatures (see Supporting Information for more details). The obtained $P-T$ phase diagram (Figure 3) shows that rising temperature stabilizes the two ionic solid phases of NH_7 at higher transition pressures than those at 0 K. Hydrogen atoms deviate from their initial positions at higher temperatures, leading to the forming of a superionic phase that contain part-solid and part-liquid structural character, where the nitrogen ions crystallize and the hydrogen ions float around freely within the nitrogen lattice (Figure S5). The appearance of the superionic $P4_12_2$ phase is achieved at higher temperatures, indicating that ionic $P4_12_2 \text{NH}_7$ is a promising candidate structure for ammonia hydride in a wide range of pressure conditions. The superionic phase will finally break down into liquid state with increasing disorder (entropy) by the temperature effect (Figure S5), and NH_7 is tougher to melt than NH_3 and H_2 at high pressure (>55 GPa). Our results reveal that the ionic and superionic phases of NH_7 are within the reach of high-pressure synthesis in the laboratory. Although the stable temperature regions are much lower than the isentropes in temperature for Uranus/

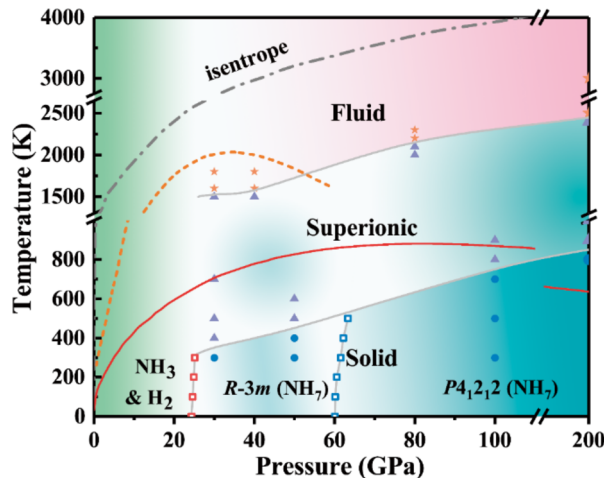


Figure 3. P – T phase diagram of NH_7 ammonia hydrides. The dashed orange line, red solid line, and dark-gray dash-dotted line represent melting lines of NH_3 and H_2 and the isentrope of Uranus/Neptune, respectively.^{30–32} The light-gray solid lines indicate phase boundaries, and the symbols are calculated data points.

Neptune (2000–7000 K), the present findings still advance fundamental knowledge about new structures and physics to address such reaction, process, and resulting products near the adiabats inside the giant planets that have important implications for planetary modeling. Furthermore, the temperature induced phase transformation between the superionic phases (favorable for releasing hydrogen) and crystal phases (favorable for storing hydrogen) provides new insights for exploring new hydrogen storage materials.

Ammonia is known to be able to accept protons and form stable ionic phases under pressure, as in, e.g., ammonium hydroxide (NH_4^+OH^-) in $P4/nmm$ symmetry, ammonium oxide ($(\text{NH}_4^+)_2\text{O}^{2-}$) in *Amma* symmetry, and ammonium amide ($\text{NH}_4^+\text{NH}_2^-$) in *Pma2* symmetry, which are predicted to become energetically stable at 3,³³ 65,³⁴ and 90 GPa,²⁶ respectively. Such novel ionic phases have been confirmed by subsequent experimental measurements.^{35,36} To probe the evolution of chemical bonding patterns of NH_7 at high pressure, we calculated the Bader charge based on the AIM theory.³⁷ Results listed in Table SII show that these ionic NH_7 structures are characterized by intriguing charge transfer behaviors among their respective constituents.

Above 25 GPa, a pressure induced dissociation of H_2 molecule occurs in NH_7 with two ammonias accepting an H^+ and forming the $\text{NH}_3\text{--H}^+\text{--NH}_3$ unit. The forming of ionic bonding between the $\text{NH}_3\text{--H}^+\text{--NH}_3$ and H^- units in the $R\bar{3}m$ structure is identified by a significant transfer of Bader charge between H^+ in $\text{NH}_3\text{--H}^+\text{--NH}_3$ (middle site) and H^- unit. The resulting hydrogen bridge bonding in the cationic group is highly unusual compared to the previously reported $P2_12_12_1$ ammonium hydroxide and *Pma2* ammonium amide as well as the $P4_12_12$ NH_7 structure studied in the present work. However, the same motif has been reported to emerge in ammonia-rich water–ammonia mixtures, where it is stabilized by proton transfer from H_2O above 60 GPa.³⁸

Even more striking is the formation of centrosymmetric bonds in $\text{NH}_3\text{--H}^+\text{--NH}_3$ with a collinear $\text{N}\text{--H}^+\text{--N}$ bonding pattern (Figure 2a), which is rare in bulk crystals; previous works on ammonia salts have identified the N_2H_7 motif, but always in a symmetry-broken $\text{NH}_4^+\text{--NH}_3$ state (the bridging

proton is not at the center).^{39–42} Here, the bridging H atom locates at the crystallographic symmetric center and is equally shared by two chemically identical units. Both $\text{N}\text{--H}$ distances of the hydrogen bridge bonds are identical at 1.228 Å, which is longer than that of the $\text{N}\text{--H}$ bond (1.018 Å) in the NH_3 unit at 50 GPa. Here, the bridge bonding is weaker than the terminal bonding, stemming from the insufficient electron localization in the hydrogen bridge bonds. Chemically speaking, it is unfavorable to form the $\text{N}\text{--H}^+\text{--N}$ unit due to the significantly different chemical bonding strength between the covalent bonds and hydrogen bonds. The novel chemical bonding observed in the present case can also be considered as a hydrogen atom forming two covalent bonds (Figure 2a) with a bond order of $s = 1/2$.⁴³ This surprising centrosymmetric bond in the $R\bar{3}m$ phase highlights significant modulation of the bonding environment in ammonia hydrides at high pressure.

As shown in Figure 2c, six equivalent bonding connections exist between the H^- and $\text{NH}_3\text{--H}^+\text{--NH}_3$ units in the $R\bar{3}m$ phase. This bonding configuration is an anion coordination, constituting anions and anion receptors. In general, most anion receptors have amide type⁴⁴ or imidazolium groups⁴⁵ as binding sites, forming $\text{N}\text{--H}\cdots\text{anion}$ or $\text{C}\text{--H}\cdots\text{anion}$ hydrogen bonds, respectively.⁴⁶ Interestingly, in the current case, H^- occupies the anion position, which has not been previously reported. The $\text{N}\text{--H}$ and $\text{H}\cdots\text{H}^-$ distances are 1.018 and 1.498 Å at 50 GPa, respectively. The $\text{N}\text{--H}\cdots\text{H}^-$ hydrogen bond strength is slightly weaker than that in H_2O but is stronger than that in ammonia, judged by the distance of $\text{H}\cdots\text{O}$ in H_2O (1.409 Å)⁴⁷ and of $\text{H}\cdots\text{N}$ in ammonia (1.702 Å)⁴⁸ at the identical compression condition. The theoretical bond energy⁴⁹ of $\text{H}\cdots\text{H}^-$ is 10.26 kJ/mol in the $R\bar{3}m$ phase at 50 GPa (Figure S6a), which is comparable to the results for typical hydrogen bonds. Furthermore, we analyzed the bonding behavior using the bond critical points (BCPs) derived from a QTAIM analysis (Figure 4).^{50,51} The BCP between H^- and the nearest terminal H in the N_2H_7^+ unit possesses an electron density ρ of 0.03 au and a positive Laplacian of 0.06 au. The positive Laplacian and small value of electron density are indicative of the hydrogen-bonded nature for the $\text{N}\text{--H}\cdots\text{H}^-$ bonding.⁵² The typical dihydrogen bond,⁵³

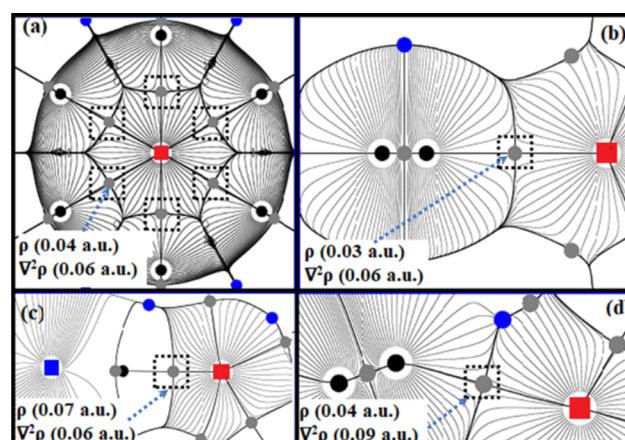


Figure 4. Gradient paths and critical points derived from a QTAIM analysis for NH_7 in (a, b) the $R\bar{3}m$ phase at 50 GPa and (c, d) the $P4_12_12$ phase at 100 GPa. Gray spheres represent BCPs, black spheres represent H , and red squares represent H^- . Gray spheres in dashed-line boxes represent BCPs between (a) H^- and N_2H_7^+ , (b) H^- and H_2 , (c) H^- and NH_4^+ , and (d) H^- and H_2 .

$X-H^{+\delta-\delta}H-Y$, involves a weak acid hydrogen bond as a proton donor, $X-H^{+\delta}$, and a negatively polarized hydrogen atom in δ^-H-Y acting as a proton acceptor.⁵⁴ In comparison to the typical situation, the H^- anion emerged from the split hydrogen molecule in the present case can be considered as a proton receptor in the $R\bar{3}m$ phase rather than a hydrogen atom polarized by Y, a less electronegative element than H. In this view, the $N-H\cdots H^-$ bond can be regarded as a special dihydrogen bond. As pressure further increases above 60 GPa, each of the NH_3 molecules in the NH_7 structure accepts a proton from H_2 , forming another ionic phase with $P4_{1}2_{1}2$ symmetry composed of NH_4^+ , H^- , and H_2 units. As depicted in Figure 2e, the NH_4^+ cation connects with the H^- anions at three distances of 1.155, 1.192, and 1.279 Å at 100 GPa, and the resulting bond energy of the $H\cdots H^-$ component among $N-H\cdots H^-$ is 76.11 kJ/mol (Figure S6b). These results indicate a considerably enhanced ability of the NH_3 unit to accept a proton at the higher pressures, which is a key driving force for the phase transition.

Bader analysis indicates very small charge transfer from the ionic species to the H_2 molecules, and H_2 is basically neutral (Table S2). The H_2 is needed to fill voids in the ionic $(NH_4^+)H^-$ structure because the two ionic species have very different sizes,⁵⁵ thus, packing of $(NH_4^+)H^-$ alone (global stoichiometry NH_5) is not efficient, and only with additional H_2 in the structure does it become favorable under pressure. An alternative probe of the vibrational properties of NH_7 confirms that the interactions between the ionic species and the H_2 molecules are weak (see the Supporting Information).

To further elucidate the mechanisms for the pressure-induced phase transitions leading to the formation of the two ionic NH_7 phases, we examined the evolution of the internal energy (U) and the product of pressure and volume (PV), which contribute to the enthalpy ($H = U + PV$) of the pertinent material systems and phases in response to pressure change. We show in Figure 5a the pressure dependence of ΔU , $\Delta(PV)$, and ΔH , defined as the values for the $R\bar{3}m$ NH_7 measured relative to those for NH_3+2H_2 , which are set to zero. It is seen clearly that the phase transition from NH_3+2H_2 mixture to the $R\bar{3}m$ phase is caused by the steep decrease of the internal energy of the latter; meanwhile, the PV term of the

$R\bar{3}m$ phase rises with increasing pressure, although its large negative magnitude is still the main contributor to the overall negative relative enthalpy around the phase transition pressure. At further increasing pressures, the fast decreasing U term continues to overcompensate for the rising PV term, resulting in the stabilization of the $R\bar{3}m$ NH_7 relative to the $NH_3 + 2H_2$ mixture. These results indicate that the exotic hydrogen bonding and ionic bonding formed in the $R\bar{3}m$ phase of NH_7 are the key driving mechanisms for the phase transition and stabilization. On the other hand, both the U and PV terms make similar contributions to lowering the enthalpy (Figure 5b), therefore driving the phase transition at about 60 GPa from the $R\bar{3}m$ phase to the $P4_{1}2_{1}2$ NH_7 and maintaining the stability of the latter at higher pressures. Here, the volume reduction and additional bonding with a sequence of H_2 dissociation events in the $P4_{1}2_{1}2$ phase are equally important mechanisms for the phase transition.

We also simulated Raman, infrared spectra, and XRD patterns of $R\bar{3}m$ phase at 30 GPa and $P4_{1}2_{1}2$ phase at 70 GPa (Figure S7) as a reference point for experimental characterization. The H_2 vibron is strongly blue-shifted under pressure (reaching almost 5000 cm⁻¹ at 70 GPa), in stark contrast to what is seen in pure hydrogen. Due to the polarizing environment, the H_2 vibron should have significant IR intensity in both the $R\bar{3}m$ and $P4_{1}2_{1}2$ phases.

In summary, we performed an extensive structure search in conjunction with first-principles energetic calculations to explore the formation, stability, evolution, and phase transitions of ammonia hydrides at high pressure and high temperature. We identified two ionic phases in a novel NH_7 stoichiometry that contain exotic hydrogen bonding patterns. The first ionic phase in $R\bar{3}m$ symmetry hosts several intriguing bonding configurations, especially a highly unusual collinear $N-H^+-N$ bonding pattern in the centrosymmetric $NH_3-H^+-NH_3$ unit and a hydrogen-bonded $N-H\cdots H^-$ connecting the anionic H^- unit to the $NH_3-H^+-NH_3$ unit. At higher pressures, NH_3 molecules develop an enhanced ability to attract protons, and each NH_3 unit accepts a proton from the hydrogen molecule, producing a phase transition to the second ionic phase with $P4_{1}2_{1}2$ symmetry, which contains NH_4^+ , H_2 , and H^- structural units. Our analysis indicates that compression induced new bonding enhancement and volume reduction play crucial yet distinct roles in bringing about these phase transitions to the exquisite ionic structures with exotic hydrogen bonding patterns in these novel ammonia hydrides. These insights advance fundamental knowledge on the mechanisms underlying the new structure and physics in these remarkable compounds, which may be present inside some large planets and are within the reach of high-pressure synthesis in the laboratory. Moreover, the NH_7 compressed crystal phases possess the highest storage (33.3 wt %) and releasing (19.0 wt %) capacity of hydrogen among known materials. The temperature induced phase transformations between the superionic and crystal phases may open new avenues for designing and developing advanced hydrogen storage media.

METHODS

Our structure prediction is based on the recently developed Crystal structure AnaLYsis by Particle Swarm Optimization (CALYPSO) methodology,^{56–59} which predicts stable structures with only the knowledge of the chemical composition at given external conditions.^{3,60–62} The structural and electronic

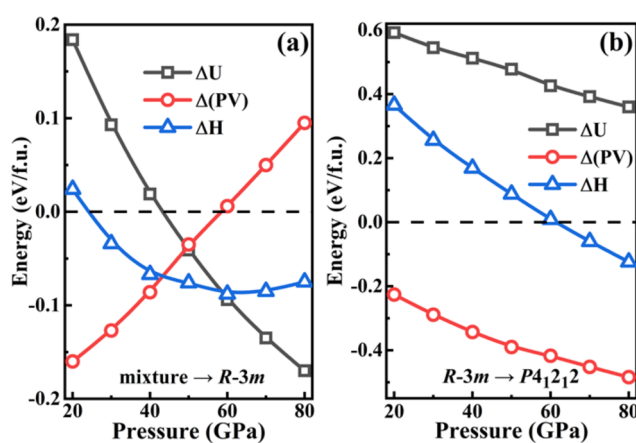


Figure 5. Calculated ΔH , ΔU , and $\Delta(PV)$ versus pressure for the predicted phase transitions: (a) $NH_3 + 2H_2$ mixture phase $\rightarrow R\bar{3}m$ phase of NH_7 and (b) $R\bar{3}m \rightarrow P4_{1}2_{1}2$ phase of NH_7 , where the mixture and $R\bar{3}m$ phase are chosen as the reference phases, respectively.

calculations were carried out using the density functional theory within the Perdew–Burke–Ernzerhof⁶³ generalized gradient approximation exchange-correlation functional as implemented in the VASP code.⁶⁴ More computational details can be found in the [Supporting Information](#).

■ ASSOCIATED CONTENT

§ Supporting Information

The Supporting Information is available free of charge on the ACS Publications website at DOI: [10.1021/acs.jpclett.9b00973](https://doi.org/10.1021/acs.jpclett.9b00973).

Computational details of the first-principles calculations, finite-temperature calculations and MD simulations, as well as the structural parameters, Bader charge, crystal structures, convex hull, phonon dispersion curves, electronic band structures, molecular structural models used for bond-energy estimates, calculated Raman, infrared spectra, and XRD patterns ([PDF](#))

■ AUTHOR INFORMATION

Corresponding Authors

*E-mail: liquan777@jlu.edu.cn.

*E-mail: chen@physics.unlv.edu.

*E-mail: mym@jlu.edu.cn.

ORCID

Ketao Yin: [0000-0002-6179-3409](https://orcid.org/0000-0002-6179-3409)

Yanchao Wang: [0000-0003-4518-925X](https://orcid.org/0000-0003-4518-925X)

Andreas Hermann: [0000-0002-8971-3933](https://orcid.org/0000-0002-8971-3933)

Hanyu Liu: [0000-0003-2394-5421](https://orcid.org/0000-0003-2394-5421)

Jian Lv: [0000-0002-6201-9888](https://orcid.org/0000-0002-6201-9888)

Quan Li: [0000-0002-7724-1289](https://orcid.org/0000-0002-7724-1289)

Author Contributions

Q.L., C.C., and Y.M. designed the project; X.S. and K.Y. performed the calculations and all authors analyzed data. X.S., K.Y., Q.L., A.H., C.C., and Y.M. wrote the paper.

Author Contributions

X.S. and K.Y. contributed equally to this work.

Notes

The authors declare no competing financial interest.

■ ACKNOWLEDGMENTS

This work was supported by the NSFC under Grants 11622432, 11404128, 11474125, and 11534003, the National Key Research and Development Program of China under Grant 2016YFB0201200, the Science Challenge Project (TZ2016001), and program for JLUT-STIRT. Part of the calculation was performed in the high-performance computing center of Jilin University and at Tianhe2-JK in the Beijing Computational Science Research Center.

■ REFERENCES

- (1) Chen, Y.; Peng, F.; Yan, Y.; Wang, Z.; Sun, C.; Ma, Y. Exploring high-pressure lithium beryllium hydrides: a new chemical perspective. *J. Phys. Chem. C* **2013**, *117*, 13879–13886.
- (2) Zhong, X.; Wang, H.; Zhang, J.; Liu, H.; Zhang, S.; Song, H.-F.; Yang, G.; Zhang, L.; Ma, Y. Tellurium hydrides at high pressures: high-temperature superconductors. *Phys. Rev. Lett.* **2016**, *116*, 057002.
- (3) Wang, H.; Tse, J. S.; Tanaka, K.; Iitaka, T.; Ma, Y. Superconductive sodalite-like clathrate calcium hydride at high pressures. *Proc. Natl. Acad. Sci. U. S. A.* **2012**, *109*, 6463–6466.
- (4) Yu, Z.; Wittbrodt, J. M.; Xia, A.; Heeg, M. J.; Schlegel, H. B.; Winter, C. H. Hydrogen and dihydrogen bonding as important features of the reactivity of the bridging hydride in pyrazolate-bridged dialuminum complexes. *Organometallics* **2001**, *20*, 4301–4303.
- (5) Qian, G.-R.; Niu, H.; Hu, C.-H.; Oganov, A. R.; Zeng, Q.; Zhou, H.-Y. Diverse chemistry of stable hydronitrogens, and implications for planetary and materials sciences. *Sci. Rep.* **2016**, *6*, 25947.
- (6) Erisman, J. W.; Sutton, M. A.; Galloway, J.; Klimont, Z.; Winiwarter, W. How a century of ammonia synthesis changed the world. *Nat. Geosci.* **2008**, *1*, 636–639.
- (7) Collin, R.; Lipscomb, W. The crystal structure of hydrazine. *Acta Crystallogr.* **1951**, *4*, 10–14.
- (8) Pimentel, G. C.; Charles, S. W.; Rosengren, K. Hydrogen Bonding of Hydrazoic Acid in Solid Nitrogen. *J. Chem. Phys.* **1966**, *44*, 3029–3033.
- (9) Goncharov, A. F.; Holtgrewe, N.; Qian, G.; Hu, C.; Oganov, A. R.; Somayazulu, M.; Stavrou, E.; Pickard, C. J.; Berlie, A.; Yen, F. Backbone NxH compounds at high pressures. *J. Chem. Phys.* **2015**, *142*, 214308.
- (10) Wang, H.; Eremets, M. I.; Troyan, I.; Liu, H.; Ma, Y.; Vereecken, L. Nitrogen backbone oligomers. *Sci. Rep.* **2015**, *5*, 13239.
- (11) Hu, A.; Zhang, F. A hydronitrogen solid: high pressure ab initio evolutionary structure searches. *J. Phys.: Condens. Matter* **2011**, *23*, 022203.
- (12) Yin, K.; Wang, Y.; Liu, H.; Peng, F.; Zhang, L. N₂H: a novel polymeric hydronitrogen as a high energy density material. *J. Mater. Chem. A* **2015**, *3*, 4188–4194.
- (13) Spaulding, D. K.; Weck, G.; Loubeyre, P.; Datchi, F.; Dumas, P.; Hanfland, M. Pressure-induced chemistry in a nitrogen-hydrogen host–guest structure. *Nat. Commun.* **2014**, *5*, 5739.
- (14) Evers, J. r.; Göbel, M.; Krumm, B.; Martin, F.; Medvedev, S.; Oehlinger, G.; Steemann, F. X.; Troyan, I.; Klapötke, T. M.; Eremets, M. I. Molecular structure of hydrazoic acid with hydrogen-bonded tetramers in nearly planar layers. *J. Am. Chem. Soc.* **2011**, *133*, 12100–12105.
- (15) Goncharenko, I.; Eremets, M.; Hanfland, M.; Tse, J.; Amboage, M.; Yao, Y.; Trojan, I. Pressure-induced hydrogen-dominant metallic state in aluminum hydride. *Phys. Rev. Lett.* **2008**, *100*, 045504.
- (16) Feng, J.; Grochala, W.; Jaroń, T.; Hoffmann, R.; Bergara, A.; Ashcroft, N. Structures and potential superconductivity in SiH₄ at high pressure: En route to “metallic hydrogen. *Phys. Rev. Lett.* **2006**, *96*, 017006.
- (17) Santra, B.; Klimeš, J.; Alfè, D.; Tkatchenko, A.; Slater, B.; Michaelides, A.; Car, R.; Scheffler, M. Hydrogen bonds and van der Waals forces in ice at ambient and high pressures. *Phys. Rev. Lett.* **2011**, *107*, 185701.
- (18) Fortes, A.; Brodholt, J.; Wood, I.; Vočadlo, L. Hydrogen bonding in solid ammonia from ab initio calculations. *J. Chem. Phys.* **2003**, *118*, 5987–5994.
- (19) Yao, Y.; Klug, D. D. Silane plus molecular hydrogen as a possible pathway to metallic hydrogen. *Proc. Natl. Acad. Sci. U. S. A.* **2010**, *107*, 20893–20898.
- (20) Zheng, M.; Cheng, R.; Chen, X.; Li, N.; Li, L.; Wang, X.; Zhang, T. A novel approach for CO-free H₂ production via catalytic decomposition of hydrazine. *Int. J. Hydrogen Energy* **2005**, *30*, 1081–1089.
- (21) Ninet, S.; Datchi, F.; Dumas, P.; Mezouar, M.; Garbarino, G.; Mafety, A.; Pickard, C.; Needs, R.; Saitta, A. Experimental and theoretical evidence for an ionic crystal of ammonia at high pressure. *Phys. Rev. B: Condens. Matter Mater. Phys.* **2014**, *89*, 174103.
- (22) Thomas, G.; Parks, G. Potential roles of ammonia in a hydrogen economy. *US Department of Energy* **2006**, 1–23.
- (23) Hubbard, W.; Nellis, W.; Mitchell, A.; Holmes, N.; Limaye, S.; McCandless, P. Interior structure of Neptune: comparison with Uranus. *Science* **1991**, *253*, 648–651.
- (24) Glaunsinger, W.; Von Dreele, R.; Marzke, R.; Hanson, R.; Chieux, P.; Damay, P.; Catterall, R. Structures and properties of metal-ammonia compounds on the trail of a new ammonia geometry. *J. Phys. Chem.* **1984**, *88*, 3860–3877.

- (25) Borstad, G.; Yoo, C. In Interactions in the ammonia-deuterium system under pressure. *J. Phys. Conf. Ser.* **2014**, *500*, 032002.
- (26) Pickard, C. J.; Needs, R. Highly compressed ammonia forms an ionic crystal. *Nat. Mater.* **2008**, *7*, 775–779.
- (27) Pickard, C. J.; Needs, R. J. Structure of phase III of solid hydrogen. *Nat. Phys.* **2007**, *3*, 473–476.
- (28) Grimme, S. Semiempirical GGA-type density functional constructed with a long-range dispersion correction. *J. Comput. Chem.* **2006**, *27*, 1787–1799.
- (29) Togo, A.; Oba, F.; Tanaka, I. First-principles calculations of the ferroelastic transition between rutile-type and CaCl_2 -type SiO_2 at high pressures. *Phys. Rev. B: Condens. Matter Mater. Phys.* **2008**, *78*, 134106.
- (30) Cruikshank, D. P.; Shapley Matthews, M.; Schumann, A. M., Eds. *Neptune and Triton*; University of Arizona Press, 1995.
- (31) Ojwang, J. G.; McWilliams, R. S.; Ke, X.; Goncharov, A. F. Melting and dissociation of ammonia at high pressure and high temperature. *J. Chem. Phys.* **2012**, *137*, 064507.
- (32) Bonev, S. A.; Schwegler, E.; Ogitsu, T.; Galli, G. A quantum fluid of metallic hydrogen suggested by first-principles calculations. *Nature* **2004**, *431*, 669–672.
- (33) Griffiths, G. I.; Misquitta, A. J.; Fortes, A. D.; Pickard, C. J.; Needs, R. J. High pressure ionic and molecular crystals of ammonia monohydrate within density functional theory. *J. Chem. Phys.* **2012**, *137*, 064506.
- (34) Robinson, V. N.; Wang, Y.; Ma, Y.; Hermann, A. Stabilization of ammonia-rich hydrate inside icy planets. *Proc. Natl. Acad. Sci. U. S. A.* **2017**, *114*, 9003–9008.
- (35) Liu, C.; Mafety, A.; Queyroux, J. A.; Wilson, C. W.; Zhang, H.; Béneut, K.; Marchand, G. L.; Baptiste, B.; Dumas, P.; Garbarino, G. Topologically frustrated ionisation in a water-ammonia ice mixture. *Nat. Commun.* **2017**, *8*, 1065.
- (36) Palasyuk, T.; Troyan, I.; Eremets, M.; Drozd, V.; Medvedev, S.; Zaleskiejgierd, P.; Magospalasyuk, E.; Wang, H.; Bonev, S. A.; Dudenko, D. Ammonia as a case study for the spontaneous ionization of a simple hydrogen-bonded compound. *Nat. Commun.* **2014**, *5*, 3460.
- (37) Tang, W.; Sanville, E.; Henkelman, G. A grid-based Bader analysis algorithm without lattice bias. *J. Phys.: Condens. Matter* **2009**, *21*, 084204.
- (38) Naden Robinson, V.; Marques, M.; Wang, Y.; Ma, Y.; Hermann, A. Novel phases in ammonia-water mixtures under pressure. *J. Chem. Phys.* **2018**, *149*, 234501.
- (39) Merlet, P.; Peyerimhoff, S. D.; Buenker, R. J. Ab initio study of the hydrogen bond in $[\text{H}_3\text{N}-\text{H}\cdots\text{NH}_3]^+$. *J. Am. Chem. Soc.* **1972**, *94*, 8301–8308.
- (40) Roziere, J.; Belin, C.; Lehman, M. S. A strong symmetrical N–H–N bond. A 120 K neutron diffraction study of hydrogen diquinuclidinone perchlorate. *J. Chem. Soc., Chem. Commun.* **1982**, 388–389.
- (41) Watt, G. W.; McBride, W. R. Ammoniates of the Ammonium Halides. *J. Am. Chem. Soc.* **1955**, *77*, 1317–1320.
- (42) Berthold, H. J.; Preibsch, W.; Vonholdt, E. On the Structure of the Cation N_2H_7^+ with an N–H···N Hydrogen Bond in the Monoammonia Adduct of Ammonium Iodide. *Angew. Chem., Int. Ed. Engl.* **1988**, *27*, 1524–1525.
- (43) Steiner, T. The hydrogen bond in the solid state. *Angew. Chem., Int. Ed.* **2002**, *41*, 48–76.
- (44) Gale, P. A. Anion coordination and anion-directed assembly: highlights from 1997 and 1998. *Coord. Chem. Rev.* **2000**, *199*, 181–233.
- (45) Chun, Y.; Singh, N. J.; Hwang, I.-C.; Lee, J. W.; Yu, S. U.; Kim, K. S. Calix [n] imidazolium as a new class of positively charged homocalix compounds. *Nat. Commun.* **2013**, *4*, 1797.
- (46) Bondy, C. R.; Gale, P. A.; Loeb, S. J. Metal–Organic Anion Receptors: Arranging Urea Hydrogen-Bond Donors to Encapsulate Sulfate Ions. *J. Am. Chem. Soc.* **2004**, *126*, 5030–5031.
- (47) Besson, J.; Pruzan, P.; Klotz, S.; Hamel, G.; Silvi, B.; Nelmes, R.; Loveday, J.; Wilson, R.; Hull, S. Variation of interatomic distances in ice VIII to 10 GPa. *Phys. Rev. B: Condens. Matter Mater. Phys.* **1994**, *49*, 12540.
- (48) Loveday, J.; Nelmes, R.; Marshall, W.; Besson, J.; Klotz, S.; Hamel, G. Structure of deuterated ammonia IV. *Phys. Rev. Lett.* **1996**, *76*, 74.
- (49) Delley, B. From molecules to solids with the DMol³ approach. *J. Chem. Phys.* **2000**, *113*, 7756–7764.
- (50) Bader, R.; Molecules, A. I. *A Quantum Theory*; Clarendon: Oxford, UK, 1990.
- (51) Vega, D.; Almeida, D. AIM-UC: An application for QTAIM analysis. *J. Comput. Methods Sci. Eng.* **2014**, *14*, 131–136.
- (52) Bader, R. F. A bond path: a universal indicator of bonded interactions. *J. Phys. Chem. A* **1998**, *102*, 7314–7323.
- (53) Richardson, T.; De Gala, S.; Crabtree, R. H.; Siegbahn, P. E. Unconventional hydrogen bonds: intermolecular B–H···H–N interactions. *J. Am. Chem. Soc.* **1995**, *117*, 12875–12876.
- (54) Bakhmutov, V. I. *Dihydrogen Bond: Principles, Experiments, And Applications*; John Wiley & Sons, 2008.
- (55) Liu, Z.; Botana, J.; Hermann, A.; Valdez, S.; Zurek, E.; Yan, D.; Lin, H.-q.; Miao, M.-s. Reactivity of He with ionic compounds under high pressure. *Nat. Commun.* **2018**, *9*, 951.
- (56) Wang, Y.; Lv, J.; Zhu, L.; Ma, Y. Crystal structure prediction via particle-swarm optimization. *Phys. Rev. B: Condens. Matter Mater. Phys.* **2010**, *82*, 094116.
- (57) Wang, Y.; Lv, J.; Zhu, L.; Ma, Y. CALYPSO: A method for crystal structure prediction. *Comput. Phys. Commun.* **2012**, *183*, 2063–2070.
- (58) Lv, J.; Wang, Y.; Zhu, L.; Ma, Y. Particle-swarm structure prediction on clusters. *J. Chem. Phys.* **2012**, *137*, 084104.
- (59) Zhang, X.; Wang, Y.; Lv, J.; Zhu, C.; Li, Q.; Zhang, M.; Li, Q.; Ma, Y. First-principles structural design of superhard materials. *J. Chem. Phys.* **2013**, *138*, 114101.
- (60) Zhu, L.; Wang, H.; Wang, Y.; Lv, J.; Ma, Y.; Cui, Q.; Ma, Y.; Zou, G. Substitutional alloy of Bi and Te at high pressure. *Phys. Rev. Lett.* **2011**, *106*, 145501.
- (61) Lv, J.; Wang, Y.; Zhu, L.; Ma, Y. Predicted novel high-pressure phases of lithium. *Phys. Rev. Lett.* **2011**, *106*, 015503.
- (62) Li, Q.; Zhou, D.; Zheng, W.; Ma, Y.; Chen, C. Global structural optimization of tungsten borides. *Phys. Rev. Lett.* **2013**, *110*, 136403.
- (63) Perdew, J. P.; Burke, K.; Ernzerhof, M. Generalized gradient approximation made simple. *Phys. Rev. Lett.* **1996**, *77*, 3865.
- (64) Kresse, G.; Furthmüller, J. Efficient iterative schemes for ab initio total-energy calculations using a plane-wave basis set. *Phys. Rev. B: Condens. Matter Mater. Phys.* **1996**, *54*, 11169.

Supporting Information

Exotic Hydrogen Bonding in Compressed Ammonia Hydrides

Xianqi Song,^{†,‡} Ketao Yin,^{†,‡} Yanchao Wang,[†] Andreas Hermann[‡], Hanyu Liu,[†] Jian Lv,[†] Quan Li,^{*,†,§} Changfeng Chen,^{*,§} and Yanming Ma^{*,†,§}

[†]State Key Laboratory of Superhard Materials, Key Laboratory of Automobile Materials of MOE, Department of Materials Science, and Innovation Center for Computational Physics Methods and Software, Jilin University, Changchun 130012, China

[‡]Centre for Science at Extreme Conditions and SUPA, School of Physics and Astronomy, The University of Edinburgh, Edinburgh EH9 3FD, United Kingdom

^{*}International Center of Future Science, Jilin University, Changchun 130012, China

[§]Department of Physics and Astronomy, University of Nevada, Las Vegas, Nevada 89154, USA

Computational details of first-principles calculations

We employ the principle of minimum free energy method based on ab initio density functional (DFT) total-energy calculations and a particle swarm optimization (PSO) (1, 2) algorithm as implemented in the CALYPSO code (3, 4). Structure searches are performed at 0, 50, 100, and 200 GPa with up to eight formula units for H₂-NH₃ system. In the first step, random structures of certain symmetry are constructed and the atomic coordinates are generated by the crystallographic symmetry operations. Then the structures are optimized to local minima by using DFT (VASP code) (5) calculations. After processing the first-generation structures, 60% of them with lower enthalpies are selected to produce the next generation structures by PSO, 40% of the structures in the new generation are randomly generated. A structure fingerprinting technique of bond characterization matrix is applied to the generated structures, so that identical structures are strictly forbidden. These procedures significantly enhance the diversity of the structures, which is crucial for the efficiency of the global search of structures.

The structural and electronic calculations are carried out using the density functional theory within the Perdew-Burke-Ernzerhof (6) generalized gradient approximation exchange-correlation functional as implemented in the Vienna Ab initio Simulation Package (VASP) code (5). The frozen-core all-electron projector-augmented wave (PAW) (7) method has been adopted, with 2s²2p³ (cutoff radius 1.5 au) and 1s¹ (cutoff radius 1.1 au) treated as valence electrons for N and H, respectively. The cutoff energy of 600 eV for the expansion of the wave functions into plane waves and fine Monkhorst-Pack k-meshes (8) have been chosen to ensure that all the enthalpy calculations are well converged to better than 1 meV/atom. The zero-point energy calculations were performed using the quasi-harmonic approximation as implemented in the Phonopy code (9), and the vdW interactions were calculated using the semi-empirical DFT-D2 vdW correction (10). Both the PBE-GGA functional and the Heyd–Scuseria–Ernzerhof (HSE) (11) hybrid functional were used to investigate the electronic structures. Infrared (IR) and Raman spectra are simulated within the framework of ab initio pseudopotential density functional perturbation theory (DFPT) (12), using norm-conserving pseudopotentials (13) with local-density approximation (LDA) in the QUANTUM ESPRESSO package (14). A 80 Ry plane wave cutoff energy and 8 × 8 × 8 Monkhorst-Pack k-meshes in the Brillouin-zone are employed. The estimated energy error in self-consistency is less than 10⁻³ a.u. Calculated XRD patterns from 20° to 60° for 2θ with a step of 0.02° adopt the Cu Kα1 radiation source ($\lambda=1.540562 \text{ \AA}$).

Computational details of finite-temperature calculations and MD simulations

To determine the phase boundaries between solid phases, we have performed calculations to determine the Gibbs free energy $G = U + PV - TS$, where U , P , V , T , and S are the internal energy, pressure, volume, temperature, and entropy, respectively. It is noted that G reduces to enthalpy ($H = U + PV$) at $T = 0$ K, which can be obtained from DFT calculations. The vibrational energy and entropy were obtained from lattice dynamic calculations using the Phonopy code. We have calculated Gibbs free energy for the $R-3m$ phase at 30, 40, and 50 GPa, $P4_12_12$ phase at 70, 80, and 90 GPa, and mixture phase of NH_3 and H_2 at 10, 15, and 20 GPa, at a temperature step of 10 K (data at a temperature step of 100 K are shown in Figure 3). At each temperature, the transition pressure points were evaluated by the horizontal ordinates of intersections from the calculated $G-P$ curves (Figure S5), allowing the construction of the $T-P$ phase diagram shown in Figure 3.

Ab initio MD simulations for NH_7 were performed within an NVT ensemble using the VASP code. We have adopted simulation supercells containing 192 ($2 \times 2 \times 3$ cells) and 512 ($2 \times 2 \times 2$ cells) atoms for the $R-3m$ and $P4_12_12$ phases, respectively. The time step in the MD simulation was 0.5 fs, and the self-consistency on the total energy was chosen to be 0.1 meV. An effective way to inspect the diffusion in a system is examining the atomic mean-square displacement (MSD), defined by

$$\text{MSD}(t) = (1/N) \sum_{i=0}^N \langle [r_i(t) - r_i(0)]^2 \rangle,$$
 where N is the total number of atoms, $r_i(t)$ is the atomic position at time t , $r_i(0)$ is the initial position of atom i , and $\langle \dots \rangle$ represents an ensemble average. We calculated the MSD of nitrogen and hydrogen atoms to assess the diffusion in the $R-3m$ and $P4_12_12$ phase at different temperatures with a 100 K temperature interval, as shown in Figure S6, to identify phase boundaries among solid, superionic and fluid phases.

Probing dynamical interactions between N₂H₇/NH₄ and H₂ units

In the main manuscript we have focused on electronic means to quantify the interaction between the ionic components of NH₇ (the appropriate combination of N₂H₇⁺, NH₄⁺, and H⁺) and the neutral molecular H₂ component. An alternative approach would be to study the influence of the H₂ sub-system on the vibrational properties of the ionic sub-system.

To this end, we have ‘switched off’ the interactions between the two by making the H₂ units quasi-infinitely heavy with a very high atomic mass ($M = 10000$ u), before calculating the phonon modes and frequencies. That way, the nuclei of H₂ are ‘clamped’ and cannot move. The neutral H₂ units then won’t be involved in collective phonons with the rest of the system, with the H₂ modes suppressed to effectively zero frequency. This results in idealized phonon dispersions of the ionic sub-system of NH₇ without the contribution of H₂ units, as shown in Figure S3. The absence of any imaginary phonon frequencies in the entire Brillouin zone for both the *R*-3*m* and *P*4₁2₁2 phases demonstrates that the interactions of neutral H₂ molecules and the ionic sub-systems in NH₇ are weak.

TABLE S1. Structural parameters of the predicted NH₇ phases at 50 GPa and 100 GPa.

Space group	Pressure (GPa)	Lattice parameters (Å)	Atom	Atomic coordinates		
				x	y	z
<i>R</i> -3 <i>m</i>	50	<i>a</i> = 4.2515	N1	0.3333	0.6667	0.7872
		<i>b</i> = 4.2515	H1	0.2099	0.7901	0.3148
		<i>c</i> = 10.1853	H2	0.0000	0.0000	0.5000
			H3	0.2615	0.1308	0.8471
			H4	0.0000	0.0000	0.0000
			N1	0.7538	0.5151	0.8644
			H1	0.3212	0.0685	0.0439
<i>P</i> 4 ₁ 2 ₁ 2	100	<i>a</i> = 5.4957	H2	0.0708	0.5975	0.7173
		<i>b</i> = 5.4957	H3	0.6454	0.4005	0.9584
		<i>c</i> = 5.5116	H4	0.3334	0.5834	0.7827
			H5	0.3739	0.1242	0.2464
			H6	0.1773	0.9082	0.2806
			H7	0.6794	0.6698	0.1897

TABLE S2. Calculated Bader charge on the anion and cation sites in the *R*-3*m* and *P*4₁2₁2 phases of NH₇. * δ is defined as the charge transfer from cation to anion.

	Pressure (GPa)	Ions	Charge value (e)	$\delta(e)^*$
<i>R</i> -3 <i>m</i>	50	NH ₃ –H ⁺ –NH ₃	16.42	– 0.58
		H [–]	1.48	+ 0.48
		3H ₂	6.10	+ 0.10
<i>P</i> 4 ₁ 2 ₁ 2	100	NH ₄ ⁺	8.51	– 0.49
		H [–]	1.44	+ 0.44
		H ₂	2.05	+ 0.05

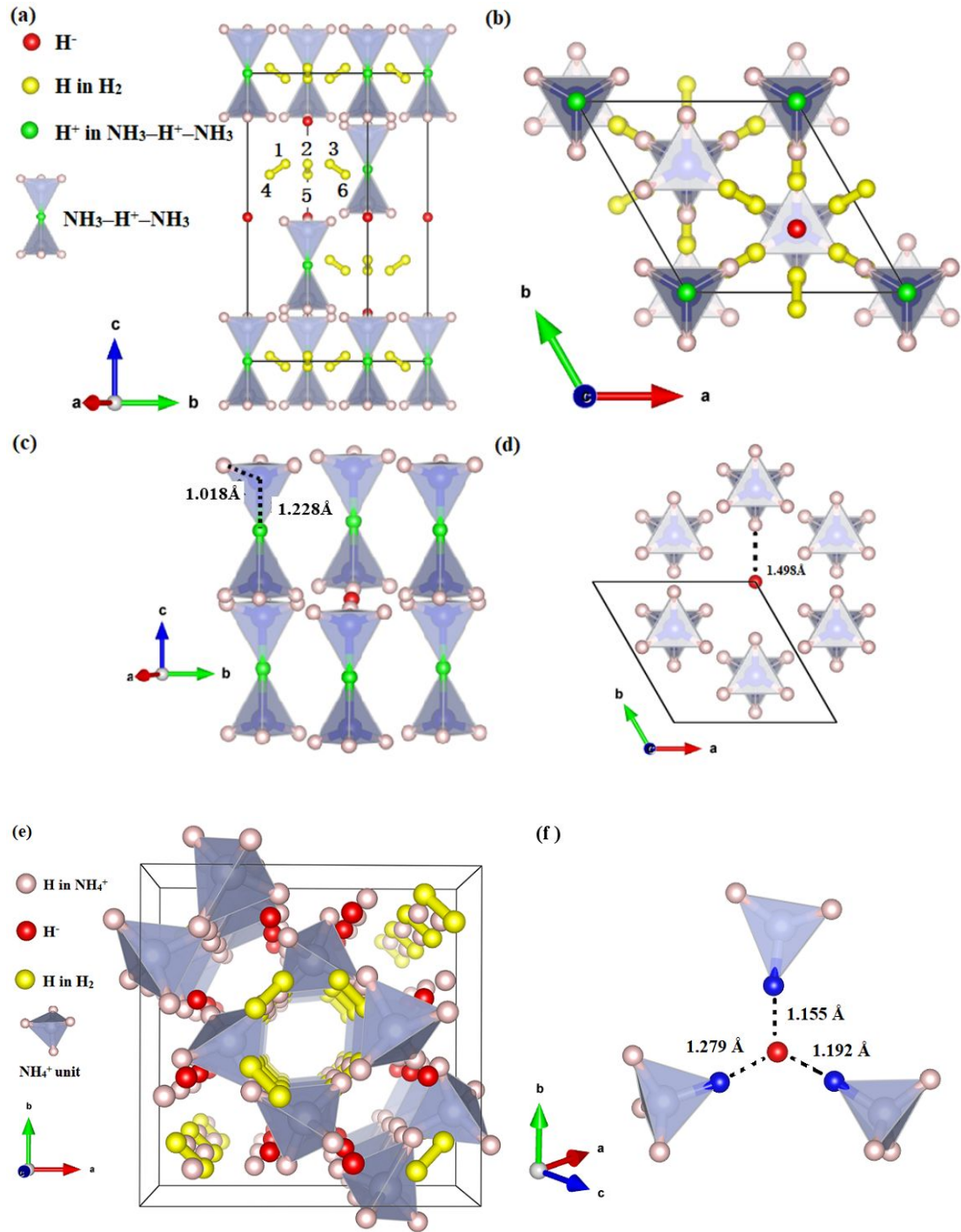


Figure S1. (a, b) Polyhedral and top view of the $R\text{-}3m$ structure of NH_7 at 50 GPa. (c,d) Hydrogen bonds between the ionic hydrogen H^- and $\text{NH}_3\text{--H}^+\text{--NH}_3$. (e) Top view of the $P4_12_12$ phase at 100 GPa. (f) The bonding characters between ionic H^- and NH_4^+ .

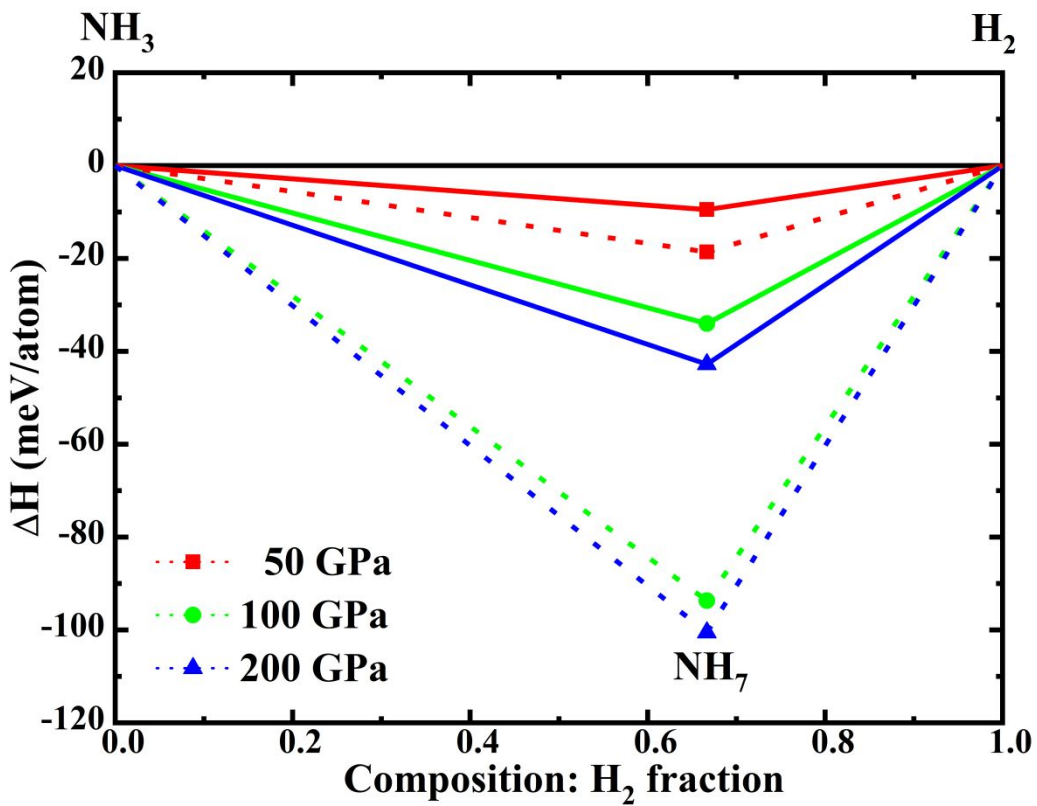


Figure S2. The calculated convex hull of the $\text{NH}_3\text{-H}_2$ systems at 50 GPa, 100 GPa, and 200 GPa. The solid lines represent the results from the standard DFT calculations and the dotted lines represent the results from DFT calculations with the inclusion of the van der Waals interaction and zero-point energy.

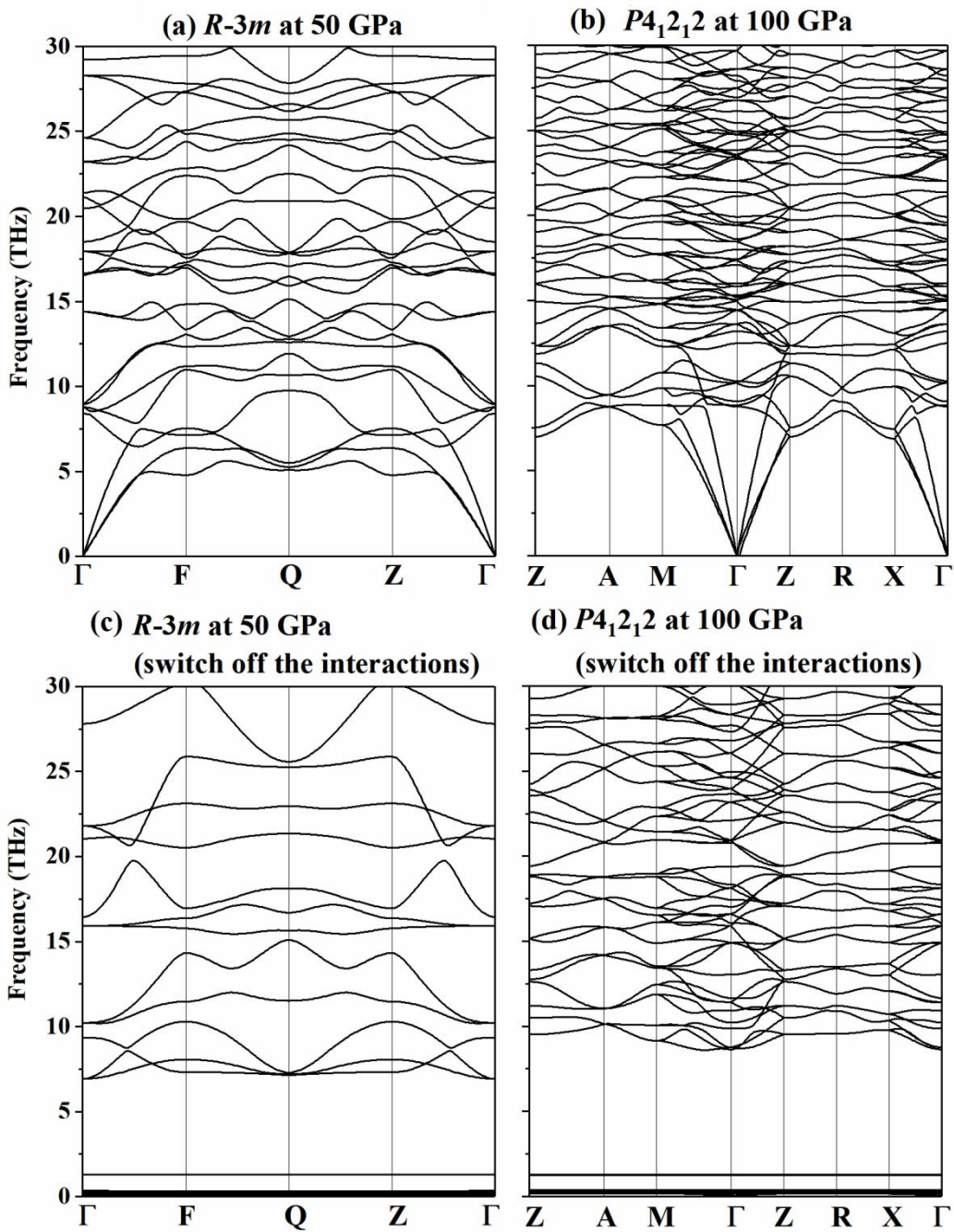


Figure S3. Calculated phonon dispersion curves of NH_7 for the $R\text{-}3m$ phase at 50 GPa and $P4_12_12$ phase at 100 GPa (a, b). Idealized phonon dispersions with clamped H_2 molecules for both phases (c, d).

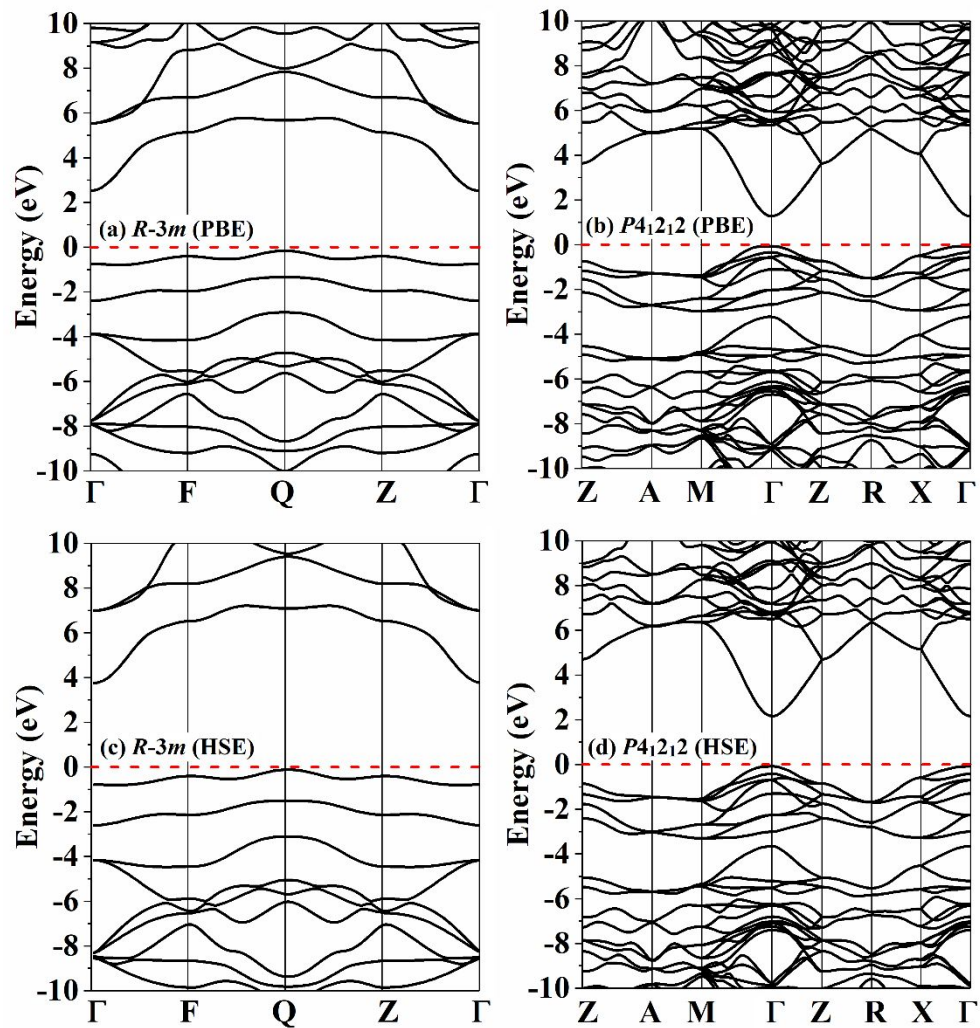


Figure S4. Calculated electronic band structures obtained using the PBE-GGA or HSE exchange-correlation functional of the *R*-*3m* phase at 50 GPa (a, c) and *P*₄₁₂₁₂ phase at 100 GPa (b, d). Dashed red lines represent the Fermi level.

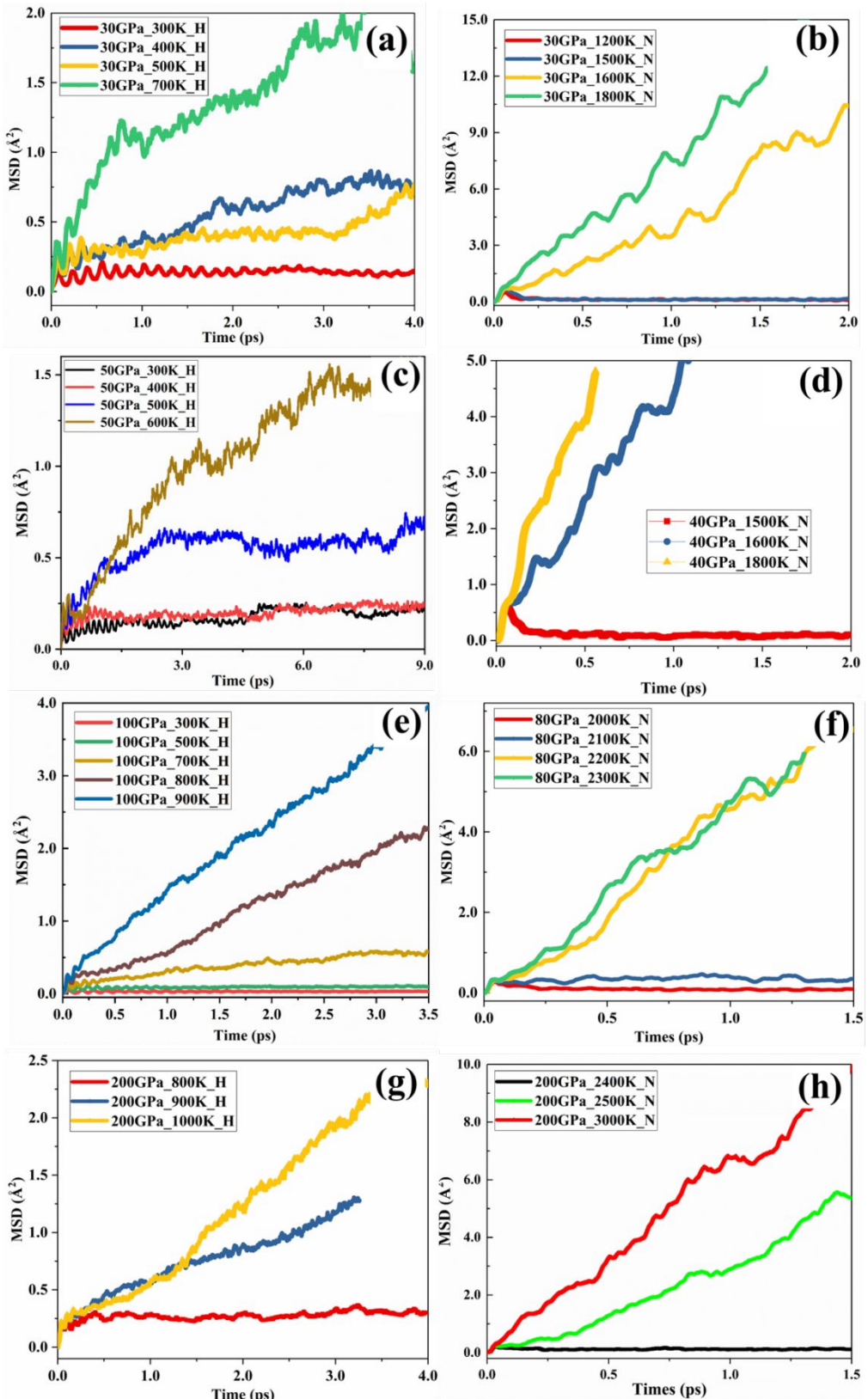


Figure S5 Mean-square displacements (MSD) as a function of time for the *R*-3*m* phase (a-d) and *P*4₁2₁2 phase (e-h) at different pressure and temperature conditions.

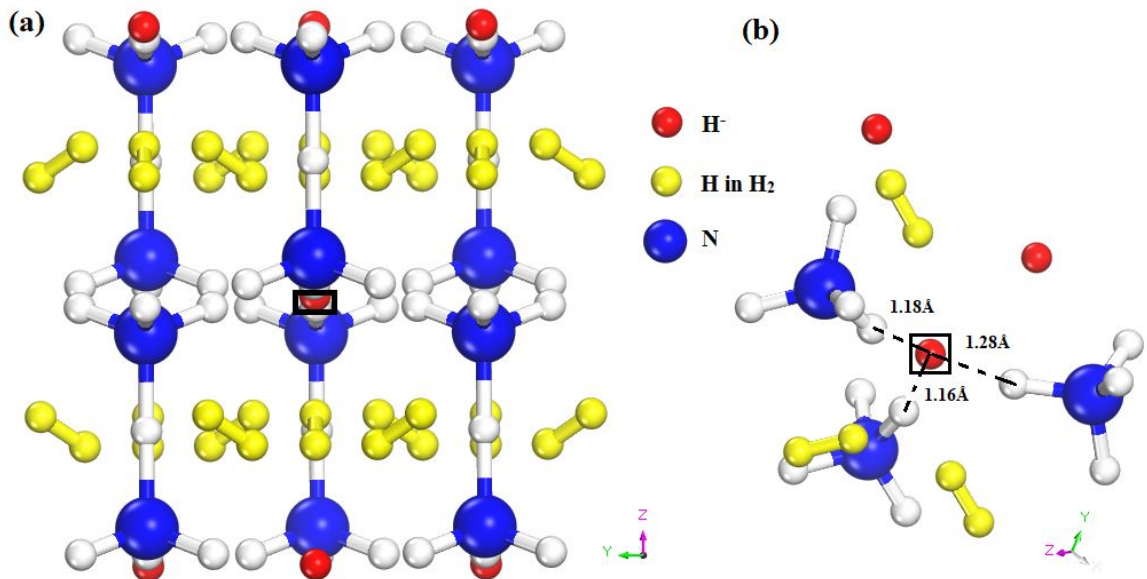


Figure S6. The molecular structural models extracted from the crystalline stable structures at (a) 50 GPa and (b) 100 GPa to estimate the N-H...H⁻ bond energy. These two molecular structural models are separated into two parts, namely the H⁻ anion enclosed in the solid rectangle and the rest. The bond energy of the H..H component among N-H...H⁻ is defined as the energy difference $\Delta E = [E(\text{total}) - E(\text{rest}) - E(H^-)]/n$, where n is the coordination number of the H⁻ anion.

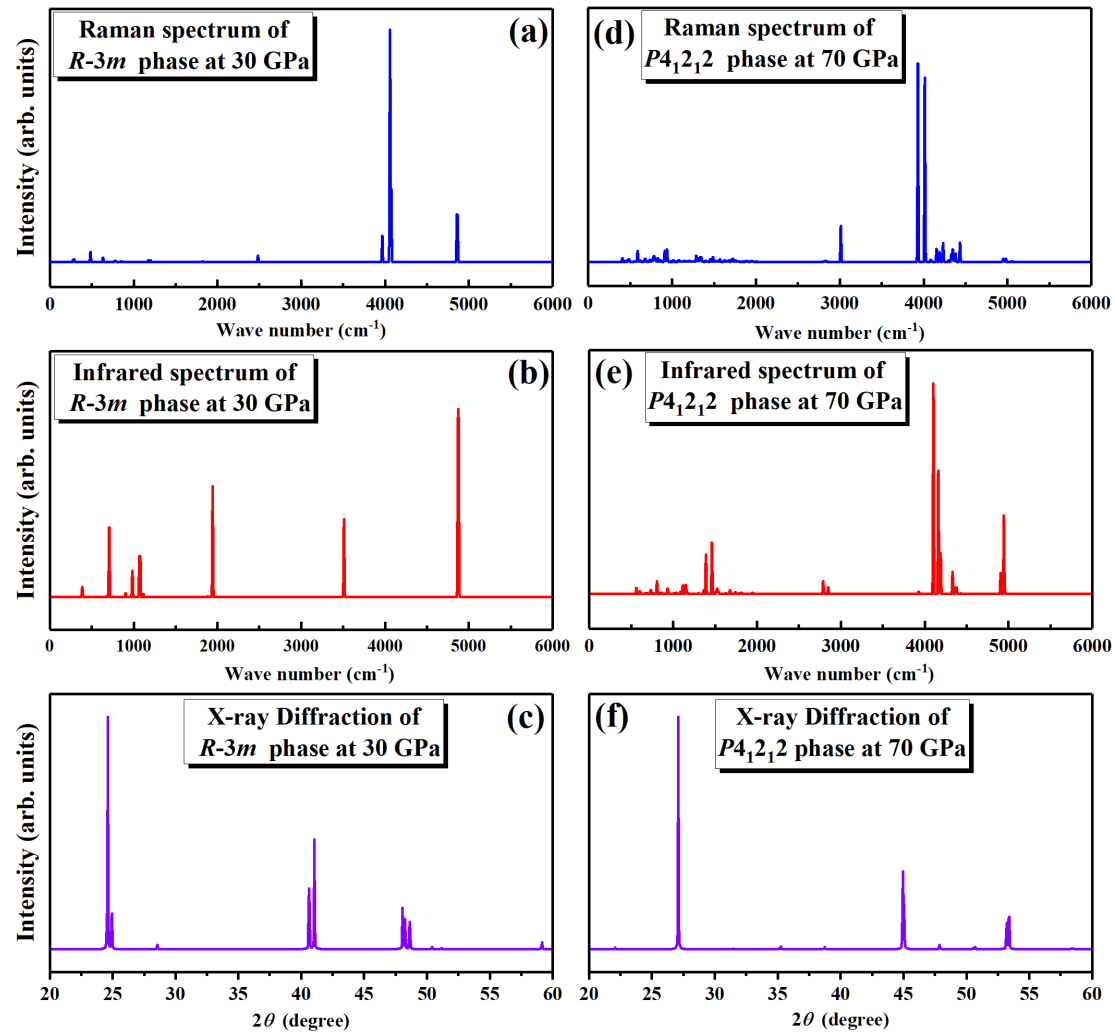


Figure S7. Calculated Raman, infrared spectra and XRD patterns of *R*-3 m phase (a-c) at 30 GPa and $P4_12_12$ phase (d-f) at 70 GPa.

References

1. Kennedy, J.; Eberhart, R. Particle Swarm Optimization, *IEEE, Piscataway, NJ*, **1995**, p. 1942.
2. Eberhart R.; Kennedy J. A New Optimizer Using Particle Swarm Theory, *IEEE, New York, NY*, **1995**.
3. Wang, Y.; Lv, J.; Zhu, L.; Ma, Y. Crystal structure prediction via particle-swarm optimization. *Phys. Rev. B* **2010**, *82*, 094116.
4. Wang, Y.; Lv, J.; Zhu, L.; Ma, Y. CALYPSO: A method for crystal structure prediction. *Comput. Phys. Commun.* **2012**, *183*, 2063-2070.
5. Kresse, G.; Furthmüller, J. Efficient iterative schemes for ab initio total-energy calculations using a plane-wave basis set. *Phys. Rev. B* **1996**, *54*, 11169-11186.
6. Perdew, J. P.; Burke, K.; Ernzerhof, M. Generalized gradient approximation made simple. *Phys. Rev. Lett.* **1996**, *77*, 3865-3868.
7. Blöchl, P. E. Projector augmented-wave method. *Phys. Rev. B* **1994**, *50*, 17953-17979.
8. Monkhorst, H. J. Special points for Brillouin-zone integrations. *Phys. Rev. B* **1976**, *13*, 5188-5192.
9. Togo, A.; Oba, F.; Tanaka, I. First-principles calculations of the ferroelastic transition between rutile-type and CaCl₂-type SiO₂ at high pressures. *Phys. Rev. B* **2008**, *78*, 134106.
10. Grimme, S. Semiempirical GGA-type density functional constructed with a long-range dispersion correction. *J. Comput. Chem.* **2006**, *27*, 1787-1799.
11. Heyd, J.; Scuseria, G. E.; Ernzerhof, M. Hybrid functionals based on a screened Coulomb potential. *J. Chem. Phys.* **2003**, *118*, 8207-8215.
12. Baroni, S.; De Gironcoli, S.; Dal Corso, A.; Giannozzi, P. Phonons and related crystal properties from density-functional perturbation theory. *J. Rev. Mod. Phys.* **2001**, *73*, 515-562.
13. Hamann, D.; Schlüter, M.; Chiang, C. Norm-conserving pseudopotentials. *J. Phys. Rev. Lett.* **1979**, *43*, 1494-1497.
14. Giannozzi P; *et al.* QUANTUM ESPRESSO: a modular and open-source software project for quantum simulations of materials. *J. Phys. Condens. Matter.* **2009**, *21*, 395502.